High Power Laser Science and Engineering, (2023), Vol. 11, e73, 6 pages.
doi:10.1017/hpl.2023.68

HIGH POWER LASER SCIENCE AND ENGINEERING

RESEARCH ARTICLE

Thulium-doped all-PM fiber chirped pulse amplifier delivering 314 W average power

Bo Ren[1], Can Li[1], Tao Wang[1], Kun Guo[1], Jian Wu[1,2,3], and Pu Zhou[1]

[1] *College of Advanced Interdisciplinary Studies, National University of Defense Technology, Changsha, China*

[2] *Nanhu Laser Laboratory, National University of Defense Technology, Changsha, China*

[3] *Hunan Provincial Key Laboratory of High Energy Laser Technology, National University of Defense Technology, Changsha, China*

(Received 25 June 2023; revised 28 July 2023; accepted 4 August 2023)

Abstract

A high-power all polarization-maintaining (PM) chirped pulse amplification (CPA) system operating in the 2.0 μm range is experimentally demonstrated. Large mode area (LMA) thulium-doped fiber (TDF) with a core/cladding diameter of 25/400 μm is employed to construct the main amplifier. Through dedicated coiling and cooling of the LMA-TDF to manage the loss of the higher order mode and thermal effect, a maximum average power of 314 W with a slope efficiency of 52% and polarization extinction ratio of 20 dB is realized. The pulse duration is compressed to 283 fs with a grating pair, corresponding to a calculated peak power of 10.8 MW, considering the compression efficiency of 88% and the estimated Strehl ratio of 89%. Moreover, through characterizing the noise properties of the laser, an integrated relative intensity noise of 0.11% at 100 Hz−1 MHz is obtained at the maximum output power, whereas the laser timing jitter is degraded by the final amplifier from 318 to 410 fs at an integration frequency of 5 kHz to 1 MHz, owing to the self-phase modulation effect-induced spectrum broadening. The root-mean-square of long-term power fluctuation is tested to be 0.6%, verifying the good stability of the laser operation. To the best of our knowledge, this is the highest average power of an ultrafast laser realized from an all-PM-fiber TDF-CPA system ever reported.

Keywords: chirped pulse amplification; high average power; thulium-doped fiber laser; ultrafast laser

1. Introduction

Over the last decade, the fiber laser community has witnessed the impressive progress of high-power ultrafast fiber lasers in the near-infrared band, mostly facilitated by the fast development of large mode area (LMA) ytterbium-doped fiber and relevant components that can be exploited with the well-known chirped pulse amplification (CPA) scheme, as well as driven by various applications[1–7]. For some applications such as special material processing, high harmonic generation, optical parametric oscillators and mid-infrared broadband supercontinuum generation[8–11], not only the power scaling but also the operation wavelength extending to a longer spectral range is required.

Specifically, the CPA system that is constructed with thulium-doped fiber (TDF) has been recognized as a promising candidate for generating high average power ultrafast lasers in the 2.0 μm range[12–15]. Thanks to the cross-relaxation process when pumping at approximately 790 nm, the output power of the TDF amplifier reached a maximum of 1 kW with the well-known master oscillator power amplification (MOPA) scheme more than a decade ago[16]. Nevertheless, owing to the relatively low optical conversion efficiency (maximum ~60%) and more significant thermal effect compared with that of the ytterbium-doped counterparts, this record has not been broken since[17–19]. As for the ultrafast operation, kilowatt-level output power was realized in 2018, with the leveraging of an LMA photonic crystal TDF that was specially designed for suppressing the unwanted nonlinear effects, such as self-phase modulation (SPM) and stimulated Raman scattering[20]. Nevertheless, owing to the using of LMA fiber with a tailored structure, most of the previous demonstrations concerning high-power ultrafast TDF amplifiers were implemented with a free-space coupled configuration, leading to a compromise of the compactness and the robustness of the laser system[21–23]. In addition, due to the effects of spectral phase distortions and the thermal lens effect induced by the remarkable

Correspondence to: Can Li and Pu Zhou, College of Advanced Interdisciplinary Studies, National University of Defense Technology, Changsha 410073, China. Emails: lc0616@163.com (C. Li); zhoupu203@163.com (P. Zhou)

water vapor absorption lines at approximately 1900 nm, the amplified laser is prone to be degraded by strong beam deformation and pulse peak power reduction[24]. As such, an all-polarization-maintaining (PM) fiberized TDF amplifier is desirable for realizing reliable operation of the laser source. However, as an all-fiber system generally demands a relatively smaller diameter of the fiber for fusion splicing and a longer length for the connection, the corresponding laser density as well as the heat deposition inside the fiber core is more serious under high-power operation, resulting in more significant nonlinear effects and a lower damage threshold. At present, by using LMA-TDF with a core/cladding diameter of 25/400 μm, all-fiber ultrafast pulse amplification has been demonstrated to deliver a maximum average power of 240 W with a pulse duration of 45 ps[25,26], whereas for femtosecond lasers, power scaling with all-fiber TDF amplifiers has been stagnant at the 100 W level[27–32]. Therefore, higher average power all-fiber femtosecond pulse amplification in the 2.0 μm range still awaits further investigation.

In this work, we experimentally demonstrated a high-power all-PM-fiber CPA system by using LMA-TDF with a core/cladding diameter of 25/400 μm as the gain fiber for the main amplifier. Through temporally stretching the seed pulse to a duration of 600 ps, a laser output with average power of 314 W and polarization extinction ratio (PER) of around 20 dB before pulse compression was obtained at approximately 1960 nm. With sufficient water-cooling and an optimized coiling radius of the gain fiber, a slope efficiency of 52% was realized. Under the maximum output power, the compressed pulse width was 283 fs, corresponding to a calculated peak power of 10.8 MW, taking into account the compression efficiency of 88% and the Strehl ratio of 89%. Moreover, the timing jitter was characterized to be 410 fs with an integration frequency of 5 kHz to 1 MHz, while the relative intensity noise (RIN) was 0.11% at 100 Hz−1 MHz under the maximum output power, verifying the excellent stable operation of the laser system. To the best of our knowledge, this is the highest average power of a femtosecond laser realized from an all-PM-TDF amplifier reported to date.

2. Experimental setup

The experimental setup of the all-PM fiber amplification system is shown in Figure 1. The seed laser was a commercial mode-locked TDF oscillator based on the semiconductor saturable absorber mirror (SESAM), which emits positively chirped pulses with average power of 180 mW at the repetition rate of 80 MHz. The corresponding optical spectrum centers at 1957 nm with a 3 dB bandwidth of 46.5 nm, while the pulse duration is 3.68 ps, as shown in Figure 2. Before launching into the amplifier via an isolator, the temporal duration of the seed laser was stretched by a PM chirped fiber Bragg grating (CFBG; positive dispersion of +34.159 ps^2) to around 600 ps via a fiber circulator. Owing to the insertion loss of the circulator and the low reflectivity (15%) of the CFBG, the remaining signal power to be amplified was approximately 20 mW. Subsequently, pre-amplifier 1 constructed with 3-m-long PM-TDF with a core/cladding diameter of 9/125 μm was employed to enhance the seed power to around 300 mW, with the core-pumping of a high-power 1550 nm fiber laser via a wavelength division multiplexer.

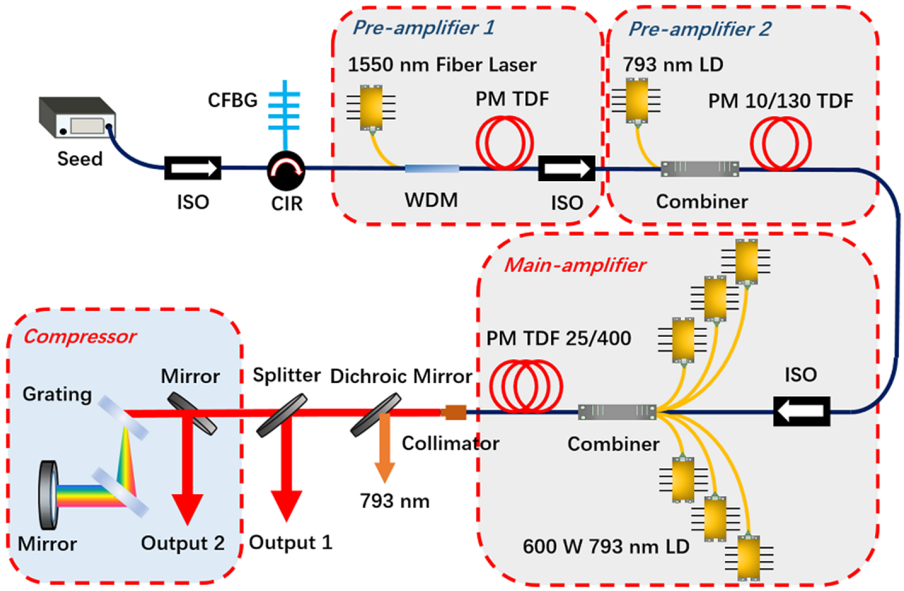

Figure 1. Experimental setup of the all-PM-TDF amplifier. LD, laser diode; ISO, isolator; CIR, circulator; CFBG, chirped fiber Bragg grating; WDM, wavelength division multiplexer.

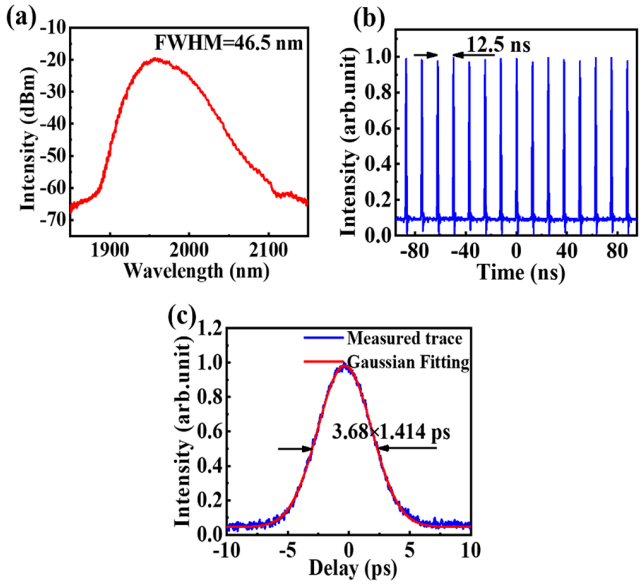

Figure 2. Output characteristics of the seed laser: (a) optical spectrum; (b) pulse train; (c) pulse duration.

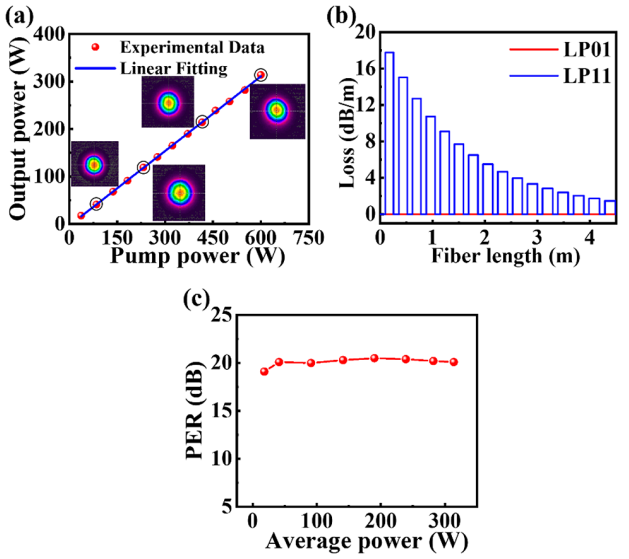

Figure 3. (a) Average power versus the pump power; inset, the monitored beam profiles under selected operation power. (b) Calculated bending loss distribution of the LP01 and LP11 modes with the runway type coiling. (c) Polarization extinction ratio (PER) versus the output power.

After that, 1.3-m-long PM-TDF with a core/cladding diameter of 10/130 μm, a core numerical aperture (NA) of 0.15 and an absorption coefficient of 4.7 dB/m at 793 nm was employed to construct pre-amplifier 2, which was cladding-pumped by a 793 nm multi-mode laser diode via a combiner. The signal power was further enhanced to approximately 5 W to guarantee enough power is injected into the main amplifier. As for the main amplifier, six commercial 793 nm laser diodes (maximum power of 100 W) were mixed with the laser signal by a $(6 + 1) \times 1$ pump/signal combiner that was connected to a 4.5-m-long commercial PM-TDF, which has a core/cladding diameter of 25/400 μm, a core NA of 0.09 and an absorption coefficient of 2.4 dB/m at 793 nm. It is noted that the length of the gain fiber was selected by considering the trade-off between the nonlinear phase shift accumulation and the amplification efficiency. The amplified laser was then output from a fiber collimator and passed through a dichroic mirror to separate it from the residual pump. Then a beam splitter was utilized to sample 10% of the amplified laser pulse for temporal de-chirping with a transmission diffraction grating pair (line density of 800 l/mm) in a folded Treacy grating compressor configuration, for the sake of avoiding damaging when compressing the laser pulse under full power. In addition, in order to avoid unwanted thermal blooming at the output of the fiber amplifier, the ambient humidity was controlled to a very low level by the employment of a dehumidifier.

3. Results and discussion

The evolution of output power with the enhancement of pump power is shown in Figure 3(a), in which the output power scales linearly without any sign of saturation. A maximum output power of 314 W was obtained under the pump power of around 600 W, corresponding to a single pulse energy of 4 μJ. The inset of Figure 3(a) shows the monitored beam profiles under selected operation power, and a near-fundamental Gaussian distribution even at the maximum output power can be observed from the figure. Essentially, by calculating the normalized frequency (V-value) of the employed active fiber in main amplifier, it can be found that there are only two transverse modes (LP01 and LP11) that could be transmitted inside the core of the fiber. To suppress the LP11 mode, the active fiber was coiled in a runway type with a minimum diameter of 10 cm and a spacing of 2 mm, with the signal launching into the fiber through the inner ring. The transmission loss of the transverse modes was calculated based on Fraunhofer's diffraction theory[33], and the results are shown in Figure 3(b). It can be observed that the loss of the LP11 mode monotonically decreases with the increasing of the diameter, and a total loss of 14.5 dB along the active fiber was estimated. Meanwhile, for the LP01 mode, even at the minimum coiling diameter there are no apparent transmission loss. It is noted that the coiling diameter was not further decreased in the experiment, as the effective mode field of the fiber would be reduced, leading to enhanced heat accumulation and nonlinear effects[19]. In addition, the beam quality factor M^2 was further theoretically estimated to be less than 1.1 based on the power proportion of each mode[34,35]. Moreover, the coiled LMA-TDF was coordinately temperature controlled with an aluminum heat sink that was water-cooled to approximately 12°C, and the runway was closely aligned with the flow direction of the

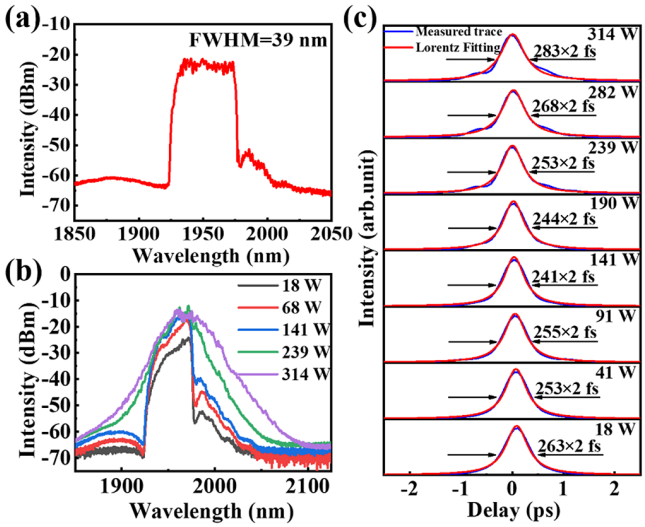

Figure 4. Spectral and temporal characteristics of the amplifier: (a) optical spectrum after pre-amplifier 2; (b) optical spectra of the main amplifier under selected output power; (c) autocorrelation traces of the de-chirped pulse under selected output power.

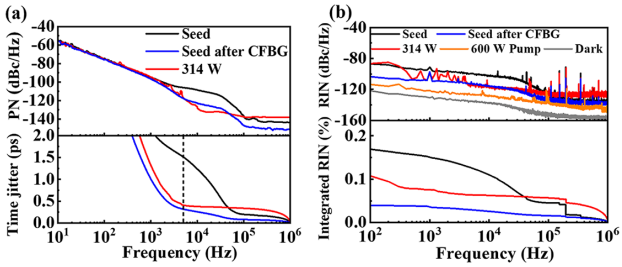

Figure 5. Noise characteristics of the seed (black line), seed filtered by the CFBG (blue line), amplified laser/pump (red/orange line) under maximum output power and the dark detection (gray line), respectively: (a) PN spectra and time jitter; (b) RIN spectra and the integrated RIN.

water to facilitate heat dissipation. In this way, a high level of slope efficiency (52%) of the main amplifier was obtained owing to the low temperature-induced stronger cross-relaxation effect[36]. The PER of the amplified laser was measured by collaboratively using a λ/2 waveplate and a polarization beam splitter (PBS) at different output powers, and the results are depicted in Figure 3(c). It can be observed that the PER remains at around 20 dB and barely changes over the power scaling process, indicating excellent stability of the all-PM-fiber CPA system.

To examine the evolution of the spectral and temporal characteristics of the laser pulse, the optical spectrum after pre-amplifier 2 was first measured and is shown in Figure 4(a). Limited by the reflection bandwidth of the CFBG, the laser spectrum was filtered and the 3 dB bandwidth was narrowed to 39 nm after the pre-amplification. Figure 4(b) demonstrates the optical spectra of the main amplifier under the selected output power. It is observed that owing to the lower gain of the TDF at the short wavelength side, the laser spectrum was apparently shaped with a steep slope at a relative low operation power, resulting in a spectral 3-dB bandwidth of 12.5 nm at the output power of 18 W. With the increasing output power, this shaping effect was slightly alleviated and the 3-dB bandwidth of the spectrum was increased to 16 nm at the output power of 141 W. Essentially, this process caused a non-trivial narrowing of the de-chirped pulse width, as shown in Figure 4(c), in which a Lorentz fitted duration of 241 fs at the output power of 141 W was realized. When the operation power was further increased, the laser spectrum gradually broadened owing to the onset of nonlinear effects, such as SPM, while the corresponding compressed pulse width was also accordingly increased with the emergence of a slight pedestal on the recorded autocorrelation traces. As an indication of the accumulated nonlinear phase shift, the maximum B-integral of the main amplifier was calculated to be 0.56π. Therefore, although the maximum available pump power has been exploited in the current experiment, further power scaling requires dedicated management of the nonlinear effects, apart from solely increasing the pump power. At the maximum output power, the center wavelength of the spectrum was 1960 nm, and the pulse width was compressed to 283 fs with a superior compression efficiency of 88% and a Strehl ratio of 89%. Regarding the spectrum components locating between 1850 and 1900 nm, they originate from the amplified spontaneous emission (ASE) at the output power of 141 W or lower, while at higher output power it slightly increased with the association of the nonlinear effects. Nevertheless, the suppression ratio of the laser signal to those spectral components is higher than 40 dB.

To characterize the noise properties of the amplified laser, the phase noise (PN) was examined in a frequency range from 10 Hz to 1 MHz by using a 12.5 GHz high-speed InGaAs photodetector and a low-noise correlation PN analyzer, and the results are shown in Figure 5(a). The measurement was carried out in single sideband mode with 50 cross-correlations and a resolution of 1% for each frequency segment. In the meantime, the RIN spectrum was measured in a frequency range from 100 Hz to 1 MHz with the employment of a signal analyzer, a 12.5 GHz photodetector and a 1.9 MHz low-pass filter that was used to avoid the detector being saturated by the signal at the repetition frequency, as shown in Figure 5(b). The noise floor of the measurement has been shown with a gray line, and is considerably lower than the recorded noise profile. As filtered by the reflection bandwidth limit of the CFBG, both the PN and the RIN of the seed were suppressed apparently; similar behaviors have also been reported in recent researches[37,38]. It is observed that the PN spectrum decreases monotonically in the frequency range lower than 5 kHz, where the noise mainly originates from the pump power variations and environmental perturbations[39]. At higher frequencies, the PN spectrum

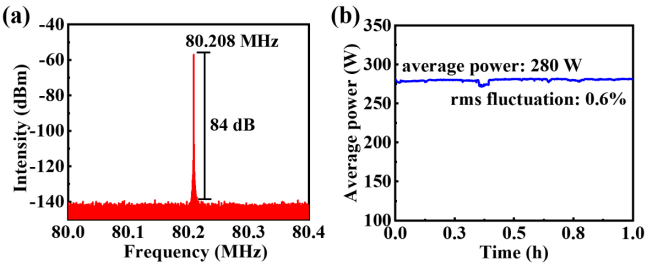

Figure 6. Stability of the amplified laser under maximum output power: (a) the radio frequency (RF) spectrum with a frequency range of 400 kHz and a resolution bandwidth (RBW) of 40 Hz; (b) output power evolution with a monitoring time of 1 hour.

of the final output at the maximum output power approaches an asymptotic level of –137 dBc/Hz, which is 13 dB higher than that of the signal after the CFBG, which is attributed to the spectrum broadening caused by the SPM effect[40]. With an integration frequency range from 5 kHz to 1 MHz, the integrated timing jitters of the input and output of the main amplifier were respectively calculated to be 318 and 410 fs, as demonstrated by the dashed line in Figure 5(a). Regarding the RIN (shown in Figure 5(b)), its increase at low frequencies (<4 kHz) after amplification is mainly attributed to the vibrations of the optical mirrors in measurement and atmospheric turbulence[20]. At higher frequencies, the RIN spectrum under maximum output power reached a plateau of –126 dBc/Hz. It can also be seen that in the examined frequency range, owing to the highly stable driver of the pump under a high driving current, the pump RIN at maximum power is even lower than the seed RIN after being filtered by the CFBG, resulting in an RIN of the amplified laser dominated by the thermal effects, ASE and external disturbances. In addition, over the examined frequency interval of 100 Hz to 1 MHz, the integrated RIN was calculated as 0.11%.

Figure 6(a) depicts the radio frequency (RF) spectrum at the fundamental repetition frequency of 80.208 MHz with a 400 kHz range and a resolution bandwidth (RBW) of 40 Hz, demonstrating a signal-to-noise ratio (SNR) of more than 80 dB. Finally, the output power stability was measured for 1 hour at output port 1 and the results are as depicted in Figure 6(b), in which the correspondingly calculated root-mean-square (rms) of the power fluctuation is as low as 0.6%.

4. Conclusion

In conclusion, we have experimentally demonstrated a Tm-doped all-PM-fiber CPA system delivering 314 W average power, corresponding to a 4 μJ pulse energy with an 80 MHz repetition rate. Through dedicated cooling and coiling of the LMA-TDF in the main amplifier, the system manifested a slope efficiency of 52% and a PER of 20 dB for the laser output. After being de-chirped by a grating pair, the pulse duration was compressed to 283 fs under the maximum output power, corresponding to a theoretical peak power of 10.8 MW, taking into account the compression efficiency of 88% and the Strehl ratio of 89%. The noise characteristics of the amplifier output were further investigated; a timing jitter of 410 fs with an integration frequency of 5 kHz to 1 MHz, and an integrated RIN of 0.11% at 100 Hz−1 MHz were respectively obtained at the maximum output power, verifying the stable operation of the laser system. Meanwhile, the long-term stable operation was further experimentally verified by monitoring the average power fluctuation, of which the rms was calculated to be 0.6%. It is believed that the demonstrated laser system can provide versatile sources for special material processing and other applications.

Acknowledgements

This work was supported by the Director Fund of State Key Laboratory of Pulsed Power Laser Technology (No. SKL2020ZR02) and the Postgraduate Scientific Research Innovation Project of Hunan Province (No. QL20210015).

References

1. F. Stutzki, F. Jansen, H.-J. Otto, C. Jauregui, J. Limpert, and A. Tünnermann, Optica **1**, 233 (2014).
2. W. S. Brocklesby, Eur. Phys. J. Spec. Top. **224**, 2529 (2015).
3. G. Chang and Z. Wei, iScience **23**, 101101 (2020).
4. J. Zuo and X. Lin, Laser Photonics Rev. **16**, 2100741 (2022).
5. T. Wang, C. Li, B. Ren, K. Guo, J. Wu, J. Leng, and P. Zhou, High Power Laser Sci. Eng. **11**, e25 (2023).
6. M. Jiang, H. Wu, Y. An, T. Hou, Q. Chang, L. Huang, J. Li, R. Su, and P. Zhou, PhotoniX **3**, s43074 (2022).
7. P. Sidorenko and F. Wise, Opt. Lett. **45**, 4084 (2020).
8. I. Mingareev, F. Weirauch, A. Olowinsky, L. Shah, P. Kadwani, and M. Richardson, Opt. Laser Technol. **44**, 2095 (2012).
9. A. Koc, C. Hauf, M. Woerner, L. von Grafenstein, D. Ueberschaer, M. Bock, U. Griebner, and T. Elsaesser, Opt. Lett. **46**, 210 (2021).
10. Q. Fu, L. Xu, S. Liang, D. P. Shepherd, D. J. Richardson, and S.-u. Alam, IEEE J. Sel. Top. Quantum Electron. **24**, 5100706 (2018).
11. C. Yao, Z. Jia, Z. Li, S. Jia, Z. Zhao, L. Zhang, Y. Feng, G. Qin, Y. Ohishi, and W. Qin, Optica **5**, 1264 (2018).
12. R. A. Sims, P. Kadwani, A. S. L. Shah, and M. Richardson, Opt. Lett. **38**, 121 (2013).
13. F. Stutzki, C. Gaida, M. Gebhardt, F. Jansen, A. Wienke, U. Zeitner, F. Fuchs, C. Jauregui, D. Wandt, D. Kracht, J. Limpert, and A. Tunnermann, Opt. Lett. **39**, 4671 (2014).
14. C. Gaida, M. Gebhardt, C. Jauregui, and J. Limpert, in *Emerging Laser Technologies for High-Power and Ultrafast Science* (2021), p. 2-1.
15. Z. Ren, F. ben Slimen, J. Lousteau, N. White, Y. Jung, J. H. V. Price, D. J. Richardson, and F. Poletti, Opt. Lett. **46**, 3013 (2021).
16. T. Ehrenreich, R. Leveille, K. Tankala, G. Rines, I. Majid, and P. Moulton, Proc. SPIE **7580**, 758016 (2010).
17. T. Walbaum, M. Heinzig, T. Schreiber, R. Eberhardt, and A. Tunnermann, Opt. Lett. **41**, 2632 (2016).

18. Y. Liu, H. Li, L. Yang, N. Dai, J. Li, C. Cao, Y. Xing, L. Liao, R. Cao, F. Zhang, Y. Chen, Y. Wang, and J. Peng, IEEE Photon. Technol. Lett. **31**, 1779 (2019).
19. X. Guan, C. Yang, Q. Gu, W. Lin, T. Tan, Q. Zhao, X. Wei, Z. Yang, and S. Xu, Appl. Phys. Express **14**, 112004 (2021).
20. C. Gaida, M. Gebhardt, T. Heuermann, F. Stutzki, C. Jauregui, and J. Limpert, Opt. Lett. **43**, 5853 (2018).
21. C. Gaida, M. Gebhardt, F. Stutzki, C. Jauregui, J. Limpert, and A. Tunnermann, Opt. Lett. **41**, 4130 (2016).
22. Z. Wang, T. Heuermann, M. Gebhardt, C. Gaida, C. Jauregui, and J. Limpert, Proc. SPIE **11260**, 112600K (2020).
23. T. Heuermann, Z. Wang, M. Lenski, M. Gebhardt, C. Gaida, M. Abdelaal, J. Buldt, M. Muller, A. Klenke, and J. Limpert, Opt. Lett. **47**, 3095 (2022).
24. M. Gebhardt, C. Gaida, F. Stutzki, S. Hadrich, C. Jauregui, J. Limpert, and A. Tunnermann, Opt. Express **23**, 13776 (2015).
25. J. Liu, C. Liu, H. Shi, and P. Wang, Opt. Express **24**, 15005 (2016).
26. Z. Zheng, D. Ouyang, X. Ren, J. Wang, J. Pei, and S. Ruan, Photon. Res. **7**, 513 (2019).
27. G. Imeshev and M. Fermann, Opt. Express **13**, 7424 (2005).
28. F. Haxsen, D. Wandt, U. Morgner, J. Neumann, and D. Kracht, Opt. Lett. **35**, 2991 (2010).
29. P. Wan, L. M. Yang, and J. Liu, Opt Express **21**, 21374 (2013).
30. F. Tan, H. Shi, R. Sun, P. Wang, and P. Wang, Opt. Express **24**, 22461 (2016).
31. J. Wu, Z. Liang, W. Lin, L. Ling, Y. Zhang, Y. Yang, X. Wei, and Z. Yang, J. Lightwave Technol. **41**, 1559 (2023).
32. Z. Ren, Q. Fu, L. Xu, J. H. V. Price, S. U. Alam, and D. J. Richardson, Opt. Express **27**, 36741 (2019).
33. D. Marcuse, IEEE J. Quantum Electron. **29**, 2957 (1993).
34. A. Kumar, R. L. Gallawa, and I. C. Goyal, J. Lightwave Technol. **12**, 621 (1994).
35. L. Yin, M. Yan, Z. Han, H. Shen, and R. Zhu, Appl. Opt. **58**, 1577 (2019).
36. P. F. Moulton, G. A. Rines, E. V. Slobodtchikov, K. F. Wall, G. Frith, B. Samson, and A. L. G. Carter, IEEE J. Sel. Top. Quantum Electron. **15**, 85 (2009).
37. W. Chen, Y. Song, K. Jung, M. Hu, C. Wang, and J. Kim, Opt. Express **24**, 1347 (2016).
38. D. Kim, S. Zhang, D. Kwon, R. Liao, Y. Cui, Z. Zhang, Y. Song, and J. Kim, Opt. Lett. **42**, 4095 (2017).
39. J. Kim and Y. Song, Adv. Opt. Photon. **8**, 465 (2016).
40. E. Poeydebat, G. Santarelli, A. Casanova, F. Scol, O. Vanvincq, G. Bouwmans, and E. Hugonnot, Opt. Lett. **46**, 2698 (2021).